

Isomer decay tagging in the heavy nuclei: ^{210}Ra and ^{209}Ra

J. J. Ressler,¹ C. W. Beausang,¹ H. Ai,¹ H. Amro,¹ M. A. Caprio,¹ R. F. Casten,¹ A. A. Hecht,¹ S. D. Langdown,^{1,2}
 E. A. McCutchan,¹ D. A. Meyer,¹ P. H. Regan,^{1,2} M. J. S. Sciacchitano,¹ A. Yamamoto,^{1,2} and N. V. Zamfir¹

¹A. W. Wright Nuclear Structure Laboratory, Yale University, New Haven, Connecticut 06520, USA

²University of Surrey, Guilford, Surrey GU2 7XH, United Kingdom

(Received 23 December 2003; published 26 March 2004)

Excited states in ^{210}Ra and ^{209}Ra were populated using the $^{184}\text{W}(^{30}\text{Si},xn)$ reaction at 148 MeV beam energy. Fusion evaporation recoils were selected using the gas-filled spectrometer, SASSYER. Prompt γ rays were detected using Compton-suppressed Ge detectors from the YRAST Ball array surrounding the target. Delayed γ rays, following isomeric decays, were detected at the focal plane of SASSYER with a smaller array of Ge detectors. The decay energy and lifetime for the $8^+(\pi h_{9/2})^n$ isomer of ^{210}Ra were determined; values for the yrast $B(E2; 8^+ \rightarrow 6^+)$ in ^{210}Ra and neighboring nuclei are interpreted within the seniority scheme. This isomer was also used to select γ -rays deexciting levels above the isomeric state in ^{210}Ra . In addition, transitions in ^{209}Ra were identified for the first time. Two high-spin isomers are suggested to exist in this isotope.

DOI: 10.1103/PhysRevC.69.034331

PACS number(s): 21.10.-k, 21.60.-n, 23.20.Lv

I. INTRODUCTION

Nuclei in the $Z \approx 82$, $N \leq 126$ region are predicted to exhibit competing structures of spherical and deformed oblate and prolate structures. The light Pb isotopes have been studied extensively, and three coexisting structures have been observed [1–9]. Similarly for nuclei with $Z < 82$ ($_{76}\text{Os}$, $_{78}\text{Pt}$, and $_{80}\text{Hg}$), coexisting weakly deformed oblate and moderately deformed prolate states have been experimentally established [10–13]. In the odd nuclei, notably ^{175}Au [14] and $^{177,179}\text{Hg}$ [15–17], spherical structures have also been identified.

Similar structures are predicted for nuclei above the $Z = 82$ shell closure; $_{84}\text{Po}$, $_{86}\text{Rn}$, and $_{88}\text{Ra}$ [18–21]. However, nuclear structure studies for these heavier nuclei have been much less conclusive. These nuclei are difficult to produce and study due to fission competition and low production cross sections. Yrast and near-yrast states of the even-even Po and Rn isotopes have been extended down to neutron numbers of 106 [22] and 112 [23], respectively. Intruder bands have been observed, but the excitation energies do not correspond to a deformed structure. With the important exception of the $0_2^+ - 2_2^+$ energy difference, the intruding band exhibits characteristics closer to an anharmonic vibrator rather than a rotor [23–26]. The heavier Ra isotopes are predicted to exhibit a deformed structure at higher neutron numbers than Po or Rn [21], but only limited structural information is available for these isotopes. The semimagic ^{214}Ra [27] and the near-magic ^{212}Ra [28] are well known, but for $A < 212$, excited states in many of these isotopes have not yet been identified.

Near the magic $N=126$ shell closure, in-beam nuclear structure experiments are also hindered by the large number of isomers present. For example, in ^{214}Ra there are six known isomers with lifetimes longer than 30 ns below 5 MeV [27]. Due to the magic neutron number, these isomers are assigned as proton excitations. Below $N=126$, only the $8^+(\pi h_{9/2})^n$ and $11^-(\pi h_{9/2} \otimes \pi i_{13/2})$ isomers are thought to persist to lower neutron numbers.

Schematic level schemes for $^{206,208}\text{Ra}$ and ^{210}Ra below the $8^+(\pi h_{9/2})^n$ isomers have been suggested by Cocks *et al.* [29], although excitation energies and transitions were not explicitly shown. A half-life of 2.24 μs was proposed for the yrast 8^+ isomer in ^{210}Ra . The presence of this isomer allows ^{210}Ra to be identified without previous knowledge of the structure. In addition, the isomeric state provides a clean “tag” to observe higher-lying excited states in ^{210}Ra using the recoil isomer decay tagging technique.

Excitation energies and decays in ^{210}Ra and ^{209}Ra are provided here for the first time. The main purpose of this paper is to highlight the structure of ^{210}Ra , with a particular emphasis on the 8^+ isomeric decay. Systematics of these $(\pi h_{9/2})^n$ isomers in the *trans*-Pb region for $N \leq 126$ are presented, and are shown to be a good example of seniority near closed shells.

II. EXPERIMENT

The experiment was performed at the Wright Nuclear Structure Laboratory, utilizing a beam of ^{30}Si accelerated to 148 MeV. Light Ra isotopes were produced following bombardment of two stacked isotopically pure targets of ^{184}W (200 $\mu\text{g}/\text{cm}^2$ each). Prompt γ transitions were detected in an array of Ge detectors which surrounded the target.

At the time of this experiment, the Ge array was comprised of eight clover HPGe detectors, of 150% relative efficiency each, from the YRAST Ball array [30]. Four detectors were placed at 90° to the beam axis, and four at the backward angle of 140° , with an overall efficiency of $\sim 2.4\%$ at 1.3 MeV.

As mentioned previously, fusion reaction studies above Pb are hindered by the large fission cross section. Therefore, to select fusion events, reaction recoils were separated in the Small Angle Separator System at Yale for Evaporation Residues (SASSYER, Ref. [31]). The gas-filled (≈ 1 Torr He) spectrometer was set to a magnetic rigidity of 1.8 T m to select fusion recoils with $A \approx 210$. The transmission efficiency of SASSYER is $\approx 15\%$ in this mass region. Contami-

nants from fission and unreacted beam particles were swept into a beam dump box located at the first dipole. To contain the gas, a thin ($50 \mu\text{g}/\text{cm}^2$) C foil was placed ~ 1 m upstream from the target chamber. The 148 MeV ^{30}Si beam lost ~ 1 MeV in this C foil before target bombardment.

Following separation, recoils were implanted into a 30-element Si solar cell array. Each solar cell covered an area of 1 cm^2 ; the entire array was 10 cm wide by 3 cm high. The solar cell array provided position, energy, and relative time information for the detection of the fusion recoils. An event in any one of the solar cell elements prompted data readout of all detectors used in this setup.

For this experiment, the recoil flight time through SASSYER was ~ 715 ns; the clover signals were therefore delayed by $1.6 \mu\text{s}$ to ensure that the signal arrived after a recoil event. Individual times (relative to a recoil implantation) for each clover were recorded and used for event-by-event Doppler correction. Prompt- γ -recoil coincidences were then selected using clover times and recoil energies corresponding to fusion-evaporation events. Overall, 5.0×10^6 recoils were detected in 105 h. Of these events, 2.3×10^6 recoil- γ_{prompt} and 0.9×10^6 recoil- $\gamma_{\text{prompt}}^n (n \geq 2)$ coincidences were collected.

Five additional HPGe detectors (of 25% relative efficiency each) were placed around the focal plane chamber, directed toward the solar cell array. Two detectors were placed at $\approx 90^\circ$, two at 45° , and one at 225° relative to the front of the solar cell array. These HPGe detectors were used to observe delayed γ decays depopulating isomeric states within $6 \mu\text{s}$ following a recoil implantation. With the 05.0×10^6 recoils, 8.7×10^4 recoil- γ_{delayed} and 0.7×10^4 recoil- $\gamma_{\text{delayed}}^n (n \geq 2)$ coincidences were collected.

III. RESULTS

Delayed transitions occurring within $6 \mu\text{s}$ following a recoil implantation are shown in Fig. 1(a). This spectrum is dominated by the 577, 601–603 doublet, 750, and 774 keV transitions. The inset shows the spectrum in a small energy range to highlight the doublet nature of the ~ 600 keV transitions.

The time difference between recoil and delayed γ events was used to measure decay half-lives of the transitions. The strongest transitions (577, 601–603, 750, 774 keV) exhibit a half-life of $2.1(1) \mu\text{s}$, determined by a weighted least-squares fit to the intensity of each transition as a function of time. These transitions are suggested to arise from the decay of the $8^+(\pi h_{9/2})^n$ isomer in ^{210}Ra . The decay curve is shown in Fig. 2. This measurement is in excellent agreement with the $2.24 \mu\text{s}$ half-life reported by Cocks *et al.* [29].

Numerous weaker transitions were also observed in the isomer detectors. Due to the low intensity and large background from the ^{210}Ra decays, half-lives for many of these transitions could not be determined in the current work. Table I lists the observed γ -ray energies and associated intensities for the delayed transitions. Intensities shown have been approximately corrected for relative efficiency. This was accomplished by placing a ^{152}Eu source near the center of the solar cell array, and making the gross assumption that

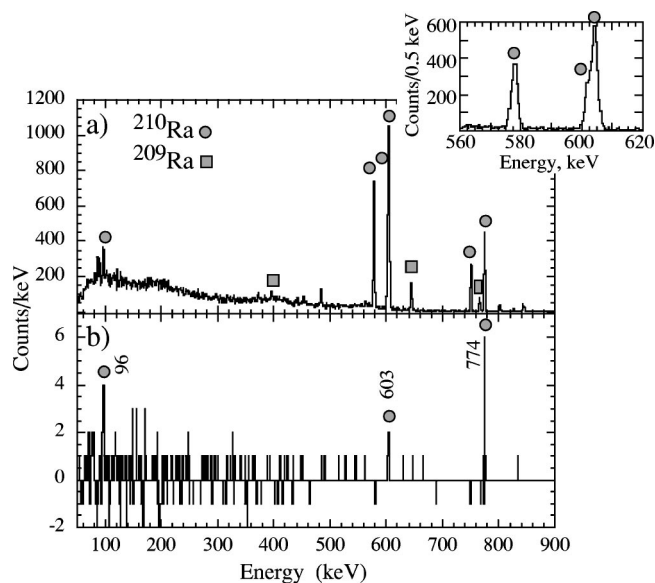


FIG. 1. (a) Delayed γ transitions observed within $6 \mu\text{s}$ following a recoil implantation in the solar cell array. The inset shows an expanded region, demonstrating the doublet nature of the 601–603 keV γ rays. (b) Coincidences with the 577 keV transition assigned to ^{210}Ra . Coincidences with 96, 603, and 774 keV γ rays are observed.

the radiation emitted from the 30 cm^2 solar cell array is similar to a point source. Low-energy γ rays were significantly attenuated by the walls of the focal plane chamber, and the intensities in Table I should be viewed as lower limits.

Coincidences between the focal plane Ge detectors were very weak for the strongest transitions, and unavailable for the weaker. For the proposed ^{210}Ra γ rays, weak coincidences were used to build the level scheme below the isomer shown in Fig. 3. The low-energy transition at 96 keV was observed in coincidence with the ^{210}Ra transitions, and is suggested to be the decay from the 8^+ isomer to the 6^+ yrast state. An example of the available statistics is shown in Fig. 1(b), where transitions coincident with the 577 keV decay energy are displayed.

Prompt γ transitions in coincidence with recoils implanted in the solar cell array are shown in Fig. 4(a). These

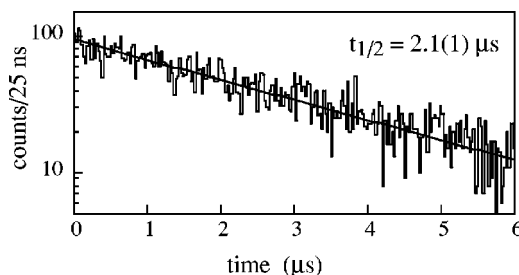


FIG. 2. Decay curve for the deexcitation of the proposed 8^+ isomer in ^{210}Ra . The summed intensity for the 577, 601, 603, 750, and 774 keV transitions is shown as a function of time following a recoil implantation in the solar cell array. Using a weighted least-squares fit, a half-life of $2.1(1) \mu\text{s}$ is suggested. The solid line shows a $2.1 \mu\text{s}$ decay half-life.

TABLE I. γ -ray energies and relative intensities observed in the isomer detectors within $6 \mu\text{s}$ of a recoil event. Also shown are multiplicities and intensities including internal conversion contributions [32] for transitions assigned to ^{210}Ra and ^{209}Ra . The isomer detectors are sensitive to half-lives within the microsecond range.

E_γ (keV)	Assigned to	I_γ^a	Multiplicity and I_{tot}^b
85.3(5)		5.8(7)	
88.6(5)		5.9(7)	
95.7(5)	^{210}Ra	9(1)	$E2$; 108(13)
126(1)		2.7(6)	
370.8(5)	^{209}Ra	3.1(7)	$M1$; 4(1)
395.6(5)		5.0(8)	
452.0(5)		3.4(8)	
482.4(5)		10(1)	
562.4(5)		5(1)	
577.1(5)	^{210}Ra	100(5)	$E2$; 100(5)
601.2(5)	^{210}Ra	59(7)	$E2$; 59(7)
603.5(6)	^{210}Ra	157(9)	$E2$; 157(9)
628.7(9)		2.8(6)	
643.6(5)	^{209}Ra	26(2)	$E2$; 26(2)
749.7(5)	^{210}Ra	59(3)	$E2$; 59(3)
765.3(5)	^{209}Ra	16(2)	$E2$; 16(2)
773.7(5)	^{210}Ra	102(5)	$E2$; 101(5)
801.2(5)		9(1)	
825(1)		2.3(4)	
842.6(6)		9(1)	

^aRelative to 577 keV transition.

^bIntensity with internal conversion corrections [36], relative to 577 keV transition.

are γ rays detected at the target position using the Ge clover array, which have the proper flight time and recoil energy for fusion-evaporation events. A large number of transitions were observed, and may be assigned to Ra and Fr isotopes

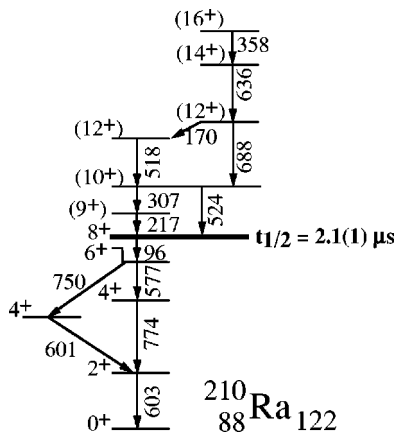


FIG. 3. Tentative level scheme for ^{210}Ra . States below the 8^+ isomer were detected in a small Ge array surrounding the Si solar cell detectors at the focal plane of SASSYER, while states above the isomer were detected in a clover Ge array surrounding the target chamber.

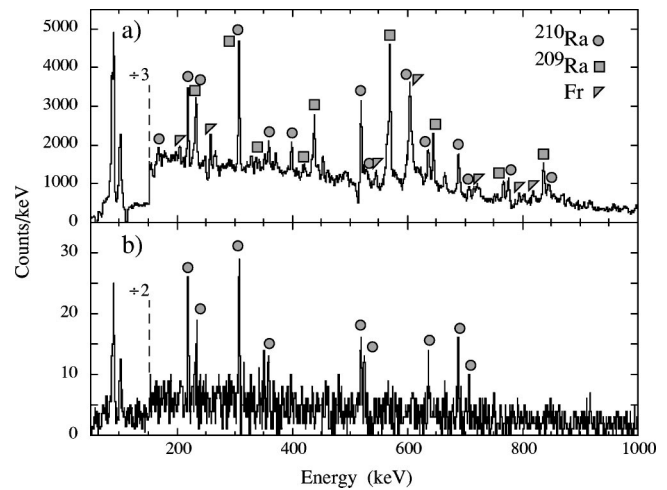


FIG. 4. (a) Prompt γ transitions measured using the clover array at the target position. Isotopes of $^{209,210}\text{Ra}$ and Fr may be assigned. Below 150 keV the spectrum is attenuated $\times 3$ to show the intense x rays on a similar scale as the γ transitions. (b) Prompt γ transitions in coincidence with delayed γ decays assigned to ^{210}Ra detected within $6 \mu\text{s}$ following a recoil implantation. Transitions above the μs isomer in ^{210}Ra are observed. As in part (a), the x-ray portion of the spectrum is attenuated ($\times 2$).

based on coincidences with x rays. Due to the limited structural information in this region, specific nuclides could not be identified from the γ -ray decay data alone.

Transitions of ^{210}Ra may be selected from the prompt spectrum by requiring prompt and delayed γ coincidences with a recoil implantation. Prompt γ transitions in coincidence with the ^{210}Ra delayed γ rays (577, 601–603, 750, and 774 keV) are shown in Fig. 4(b). Transitions in the prompt spectrum are assigned as decays from higher-spin states feeding the 8^+ isomer at 2.05 MeV.

Recoil-gated γ - γ coincidences between the prompt γ rays were then used to extend the proposed level scheme of ^{210}Ra to $\sim 16\hbar$ and 4.3 MeV excitation energy. The resulting level scheme is shown in Fig. 3. Spin and parities are suggested by comparison to the neighboring nuclides and relative γ -ray intensities between the two rings of the clover array. Quadrupole transitions will be favored in the backward ring (140°), while dipole transitions will be favored in the side ring (90°). Intensities were too weak to perform gated intensity comparisons [such as Directional Correlation Orientation (DCO) ratios]. Table II lists prompt γ -ray energies and intensities assigned to ^{210}Ra .

In addition, the $4_2^+ \rightarrow 2^+$, $4_1^+ \rightarrow 2^+$, and $2^+ \rightarrow 0^+$ transitions of ^{210}Ra were observed in the prompt γ -ray spectrum. The $6^+ \rightarrow 4_2^+$ and $6^+ \rightarrow 4_1^+$ were only weakly evident in the prompt γ - γ coincidences with low-lying ^{210}Ra transitions. This suggests that the 4^+ (and less so the 6^+) states have an alternate feeding pattern, bypassing the 8^+ isomeric state. Unfortunately, recoil- γ - γ statistics are too poor to clearly determine the deexcitation pathway crossing the isomer.

Weak transitions bypassing the 8^+ isomer have also been observed in the $N=122$ isotones ^{208}Rn and ^{206}Po . In ^{208}Rn , the low-lying 4^+ states have fragmented feeding patterns from multiple higher-lying 6^+ states which have only been observed in β decay [32].

TABLE II. Prompt γ -ray energies and relative intensities detected in the clover array. Transition intensities corrected for internal conversion when the multipolarity is known are also shown. Due to the low statistics in the coincidence spectra, transition intensities are measured from recoil-gated γ -ray singles. As peaks may have contributions from other sources, intensities listed here are upper limits. The value of “x” in ^{209}Ra is ≈ 900 keV.

	$E_\gamma(\text{keV})$	$E_x(\text{keV})$	$J_i \rightarrow J_f$	I_γ^a	Multipolarity and I_{tot}^b
^{210}Ra :					
	169.5(7)	3261	$(12^+ \rightarrow 12^+)$	7(1)	$M1$; 32(3)
	217.5(5)	2266	$(9^+ \rightarrow 8^+)$	55(2)	$M1$; 150(5)
	231.6(5)	Not placed		$<54(2)$	
	306.7(5)	2573	$(10^+ \rightarrow 9^+)$	$<116(4)$	$M1$; $<192(6)$
	358.5(5)	4255	$(16^+ \rightarrow 14^+)$	24(2)	$E2$; 26(2)
	397.7(5)	Not placed		29(2)	
	518.2(5)	3091	$(12^+ \rightarrow 10^+)$	100(4)	$E2$; 100(4)
	524.2(7)	2573	$(10^+ \rightarrow 8^+)$		$E2$
	601.2(5)	1204	$4^+ \rightarrow 2^+$	32(6)	$E2$; 32(6)
	603.5(6)	604	$2^+ \rightarrow 0^+$	105(6)	$E2$; 104(6)
	635.5(5)	3897	$(14^+ \rightarrow 12^+)$	59(2)	$E2$; 59(2)
	687.9(5)	3261	$(12^+ \rightarrow 10^+)$	64(3)	$E2$; 63(3)
	705(1)	Not placed		15(2)	
	773.7(5)	1378	$4^+ \rightarrow 2^+$	39(2)	$E2$; 38(2)
	843.7(5)	Not placed		33(2)	
^{209}Ra :					
	229.1(5)	$(1570+x)$	$(\frac{27^+}{2} \rightarrow \frac{25^+}{2})$	8(2)	$(M1)$
	(306)	$(1876+x)$	$(\frac{29^+}{2} \rightarrow \frac{27^+}{2})$		$(M1)$
	335.6(5)	$1342+x$	$(\frac{25^+}{2} \rightarrow \frac{21^+}{2})$	10(1)	$E2$; 11(1)
	370.8(5)	1015	$(\frac{11^-}{2} \rightarrow \frac{9^-}{2})$	18(1)	$M1$; 19(1)
	437.2(5)	$1005+x$	$(\frac{21^+}{2} \rightarrow \frac{17^+}{2})$	66(2)	$E2$; 67(2)
	568.5(5)	x	$(\frac{17^+}{2} \rightarrow \frac{13^+}{2})$	192(6)	$E2$; 191(6)
	643.6(5)	644	$(\frac{9^-}{2} \rightarrow \frac{5^-}{2})$	76(3)	$E2$; 75(3)
	765.3(5)	1409	$(\frac{13^-}{2} \rightarrow \frac{9^-}{2})$	31(2)	$E2$; 31(2)
	835.3(5)	Not placed		64(3)	
Fr:					
	201.9(5)			4(1)	
	203.9(5)			11(2)	
	257.1(5)			25(2)	
	544.6(5)			21(2)	
	605(1)			43(3)	
	714.4(5)			20(2)	
	792.5(5)			15(1)	
	817.2(5)			19(2)	
	905.2(5)			6(1)	

^aRelative to 518 keV transition.

^bIntensity with internal conversion corrections [36], relative to 518 keV transition.

Prompt γ rays not assigned to ^{210}Ra are suggested to predominantly arise from the odd-A Ra neighbor, ^{209}Ra . Weaker transitions, coincident with 86 keV K_α x rays, are assigned to Fr, with ^{209}Fr or ^{210}Fr being the most likely candidates. Transitions suggested to arise from Fr are very weak in this data set.

For a 10 h period, the beam energy was increased to

153 MeV, and the γ -ray intensities were compared to those observed at 148 MeV. While transitions assigned to ^{210}Ra become weaker, those assigned to ^{209}Ra and $^{(209,210)}\text{Fr}$ become more prominent, confirming our assignment. All data shown in this paper are derived from the much longer (105 h) 148 MeV beam period.

No structural information is available for the odd-A Ra

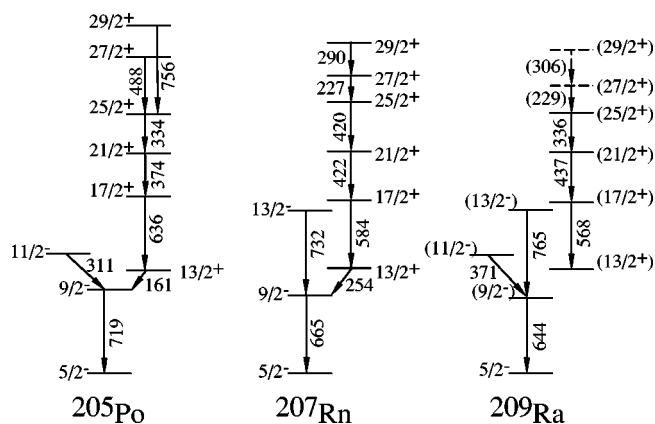


FIG. 5. Tentative level scheme for ^{209}Ra with the known level schemes for isotones ^{205}Po [47] and ^{207}Rn [48]. The $13/2^+$ states are isomeric; ^{205}Po $t_{1/2}=645(20)\mu\text{s}$ [47], ^{207}Rn $t_{1/2}=181(18)\mu\text{s}$ [47], while for ^{209}Ra the half-life is not known.

isotopes below $N=126$, with the exception of levels below a long-lived isomer in $^{213}\text{Ra}_{125}$ [33]. However, comparisons can be made to odd- A Po and Rn nuclides. These nuclei typically have low-spin negative-parity ground states ($\nu 2f_{5/2}$, $\nu 3p_{3/2}$, $\nu 3p_{1/2}$) and a long-lived $13/2^+$ ($\nu 1i_{13/2}$) isomer near 1 MeV excitation energy. Heavy-ion fusion-evaporation reactions will predominantly populate the higher-spin $13/2^+$ isomer band, which is presumed to be built on $\nu 1i_{13/2} \otimes (\pi 1h_{9/2})^2$ excitations.

γ rays observed in the prompt- γ -recoil spectrum in coincidence with 88 keV Ra K_α x rays, and not in coincidence with ^{210}Ra decays, are assigned to ^{209}Ra . Using recoil-gated γ - γ coincidences, two separate structures are observed. These are suggested to be states built on the negative-parity ground state and the $13/2^+$ isomeric state. The proposed level scheme for ^{209}Ra is shown on the far right of Fig. 5, while transition energies and intensities are shown in Table II. Spins and parities are suggested from comparisons to the $N=121$ isotones (also shown in Fig. 5) and relative intensities in the clover array rings, as was done for ^{210}Ra .

Transitions assigned to the ^{209}Ra ground state band were also observed in the isomer detectors. While the excitation energy for the $13/2^+$ isomer is not known, it is expected to lie below the $11/2^-$ and $13/2^-$ states. Therefore, a second isomer feeding the higher-lying negative-parity states is proposed.

Similar to Ra, very little information is available for the light Fr isotopes. Virtually no level schemes exist for these nuclides with $N < 124$. The strongest transitions assigned to Fr are shown in Table II.

IV. DISCUSSION

A. ^{210}Ra

The Po, Rn, and Ra isotopes with $N \sim 126$ are approximately spherical in their ground states. For the even-even nuclei, the lowest energy yrast 0^+ , 2^+ , 4^+ , 6^+ , and 8^+ states are attributed to coupling between a pair of protons in the $1h_{9/2}$ orbital. The energy difference between the 8^+ and 6^+ levels is quite small, resulting in long lifetimes for the $8^+ \rightarrow 6^+$ transitions.

The proposed half-life of $2.1(1)\mu\text{s}$ for the 8^+ isomer of ^{210}Ra agrees well with expectations. Half-lives for these isomers are observed to decrease along an isotopic chain with decreasing neutron number, and increase along an isotonic chain with increasing proton number. This would suggest a half-life of $500\text{ ns} < t_{1/2} < 11\mu\text{s}$ for ^{210}Ra by comparison to neighboring ^{212}Ra [34] and ^{208}Rn [35]. The measured half-life of $2.1(1)\mu\text{s}$ fits well within this window.

The 8^+ isomer of ^{210}Ra is suggested to decay by a single 96 keV γ ray. The amount of electron conversion can be estimated from the intensity balance of the single 96 keV γ ray feeding the 6^+ state, and the two γ rays deexciting it (577, 750 keV). This suggests a conversion coefficient of 19(2), which compares favorably with an $E2$ transition ($\alpha_{\text{calc}}=11.8$ [36]) rather than $E1$ ($\alpha_{\text{calc}}=0.12$), $E3$ ($\alpha_{\text{calc}}=320$), $M1$ ($\alpha_{\text{calc}}=3.7$), or $M2$ ($\alpha_{\text{calc}}=62.6$). Note that the 96 keV γ -ray observed intensity may be somewhat less than the true value, as low-energy transitions will be attenuated by the walls of the focal plane chamber and the efficiency is uncertain (see Results section).

Using the theoretical conversion coefficient for a pure $E2$ decay and the measured $2.1(1)\mu\text{s}$ half-life, the transition probability $B(E2; 8^+ \rightarrow 6^+)$ value is $0.035(2)$ W.u. [$2.6(2)e^2\text{ fm}^4$]. This $B(E2; 8^+ \rightarrow 6^+)$ value is much less than the known values for the isotones ^{208}Rn [$0.187(7)$ W.u. [35]] and ^{206}Po [$2.49(17)$ W.u. [37]]. The drop in $B(E2)$ values as the $\pi h_{9/2}$ orbital is filled is observed not only in the $N=122$ isotones, but for $N=124$ and $N=126$ as well. For comparison, excitation energies, decay transitions, half-lives, and transition probabilities [$B(E2)$ values] are shown in Table III for the known 8^+ isomers in the $Z > 82$, $N \leq 126$ region.

Typical behavior for $B(E2)$ values would suggest an increase, not a decrease, as the shell is filled and the proton number moves away from magicity. However, the apparently anomalous behavior of the $B(E2; 8^+ \rightarrow 6^+)$ values can be easily and elegantly explained using the seniority coupling scheme.

Seniority (ν) may be simply described as the smallest number of unpaired particles (or holes) needed to couple to a given state of spin J . The concept is generally useful for near-spherical nuclei where states are dominated by a single configuration of the type $|j^n J\rangle$. In the *trans*-Pb region with $N \leq 126$, low-energy states for the Po, Rn, and Ra nuclei are dominated by $\pi 1h_{9/2}^n$ excitations. In the seniority scheme, the 2^+ , 4^+ , 6^+ , and 8^+ states may arise from the coupling of two valence protons ($\nu=2$) in the $\pi 1h_{9/2}$ orbital. This is shown schematically on the left side of Fig. 6.

In collective nuclei higher yrast transitions are similar in character to the $2_1^+ \rightarrow 0_1^+$ transition, as all are phonon or rotational angular momentum changing transitions. The $B(E2)$ values therefore scale with each other; the $B(E2; 4_1^+ \rightarrow 2_1^+)$ is typically ~ 1.5 times larger than the $B(E2; 2_1^+ \rightarrow 0_1^+)$ value [38]. In the seniority regime, seniority conserving $J \rightarrow J-2$ transitions are fundamentally different from seniority changing transitions. This difference leads to contrasting behaviors for $B(E2)$ values as a function of nucleon number.

The even-tensor, one-body transition matrix element between two states of changing seniority ($\Delta\nu=2$) is given by [39]

TABLE III. Systematics of the 8^+ isomers in the ^{210}Ra region. Energy levels, deexcitation γ rays, half-lives, and transition probabilities are shown for the $8^+ \rightarrow 6^+$ transitions. Data are taken from Refs. [27,34–42] and this experiment.

		$E_x 8^+$ (keV)	$8^+ \rightarrow 6^+ E_\gamma$ (keV)	$t_{1/2}$	$B(E2)$ (W.u.)
$N=126$	^{210}Po	1557	83.54(8)	98.9(25)ns	1.10(5)
	^{212}Rn	1694	54.2(2)	910(30)ns	0.115(6)
	^{214}Ra	1865	45.5(5)	67(3) μs	0.00136(17)
$N=124$	^{208}Po	1528	4.02(3)	350(20)ns	6.4(5)
	^{210}Rn	1665	<50	644(40)ns	>1.57(15)
	^{212}Ra	1958	63.3(5)	10.9(4) μs	0.0079(8)
$N=122$	^{206}Po	1573	12.5(1)	222(10)ns	2.49(17)
	^{208}Rn	1828	89.9(1)	487(12)ns	0.187(7)
	^{210}Ra	2049	95.7(5)	2.1(1) μs	0.035(2)

$$\langle j^n \nu J \| O_p^{even} \| j^n \nu - 2, J' \rangle = \left[\frac{(n - \nu + 2)(2j + 3 - n - \nu)}{2(2j + 3 - 2\nu)} \right]^{1/2} \times \langle j^\nu \nu J \| O_p^{even} \| j^\nu \nu - 2, J' \rangle, \quad (1)$$

where n is the number of particles in the orbit with spin j , and ν is the seniority. In Fig. 6(a), the square of the matrix element is plotted as a function of shell filling for $j=9/2$ particles. The square of the matrix element amplitude shows the usual trend for $B(E2; 2^+ \rightarrow 0^+)$ transition probabilities. The $B(E2)$ value varies as $f(1-f)$ where f is the fractional

filling of the shell [40], reaching a maximum at midshell.

For even-tensor, one-body seniority conserving ($\Delta\nu=0$) transitions, the matrix element is given by [39]

$$\langle j^n \nu J \| O_p^{even} \| j^n \nu J' \rangle = \left(\frac{2j + 1 - 2n}{2j + 1 - 2\nu} \right) \langle j^\nu \nu J \| O_p^{even} \| j^\nu \nu J' \rangle. \quad (2)$$

The amplitude of this matrix element *decreases* as a shell is filled, crossing zero at midshell. The square of this amplitude for $j=9/2$ nucleons is also plotted in Fig. 6(a), where a parabolic shape opposite to that of the seniority nonconserving transitions is observed. This shape represents $B(E2; J \rightarrow J - 2)$ transitions for $J \neq 2$, varying as $(1 - 2f)^2$ [40] and minimizing at midshell.

Figures 6(b) and 6(c) show a comparison between calculated transition probabilities using the simple seniority scheme described above with experimental data for $\pi h_{9/2}^n$ excitations in the Po, Rn, and Ra isotones of $N=126$ and $N=122$. As the $h_{9/2}$ orbital is filled, the $B(E2; 8^+ \rightarrow 6^+)$ values decrease toward mid j shell. While $B(E2)$ values for the $N=122$ isotones are not exactly reproduced by the calculation, the general trend is the same. The broader consequences of this simple interpretation are discussed in a separate publication [41].

Since the low-energy structure of ^{210}Ra is dominated by $\pi h_{9/2}^n$ excitations as shown above, level energies are expected to be similar to neighboring nuclei. Excitation energy comparisons for the isotopes and isotones of ^{210}Ra are shown in Fig. 7. The proposed level scheme for ^{210}Ra agrees well with smooth changes along both the proton and neutron axes. The maximally aligned $h_{9/2} \nu=2$ 8^+ excitation energy and $8^+ \rightarrow 6^+$ energy difference increase as neutrons are removed from the $Z=88$ isotopes and as protons are added to the $N=122$ isotones.

All three $N=122$ isotones shown in Fig. 7 have two competing 4^+ levels at similar excitation energies. Shown in Fig. 8 are the low-spin levels of the Po, Rn, and Ra $N=122$ isotones with relative transition probabilities for decays from the $(\pi 1 h_{9/2})_{6^+}^n$ state to the 4^+ levels. The transition strength from the 6^+ proton excitation to the 4^+ levels in ^{206}Po , ^{208}Rn ,

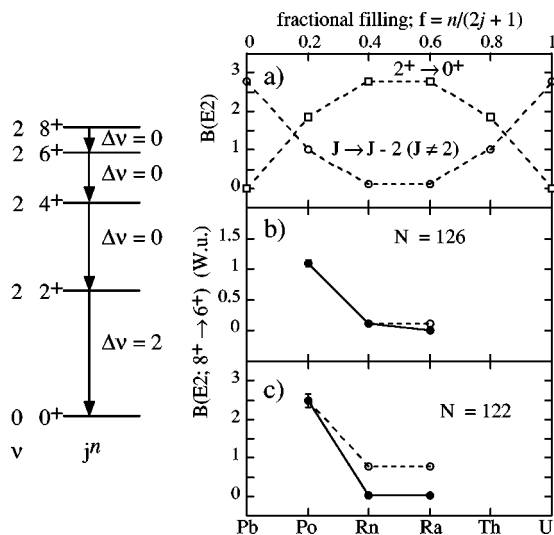


FIG. 6. On the left, a schematic diagram for excitation energies and seniority for two $j=9/2$ particles is shown. On the right are experimental and calculated [from Eqs. (1) and (2)] $B(E2)$ values. (a) Calculated $B(E2; 2^+ \rightarrow 0^+)$ values are shown as squares, while $B(E2; J \rightarrow J - 2, J \neq 2)$ values are circles. (b) Calculated (open circles) and experimental (filled circles [27,34,42]) $B(E2; 8^+ \rightarrow 6^+)$ values for the $N=126$ isotones. (c) Calculated (open circles) and experimental (filled circles [35,37], and this work) $B(E2; 8^+ \rightarrow 6^+)$ values for the $N=122$ isotones. The calculated transition probabilities are normalized to the experimental values of Po. While the $N=122$ $B(E2)$ values are not explicitly reproduced by the calculation, the trend suggests good seniority four neutrons away from magicity.

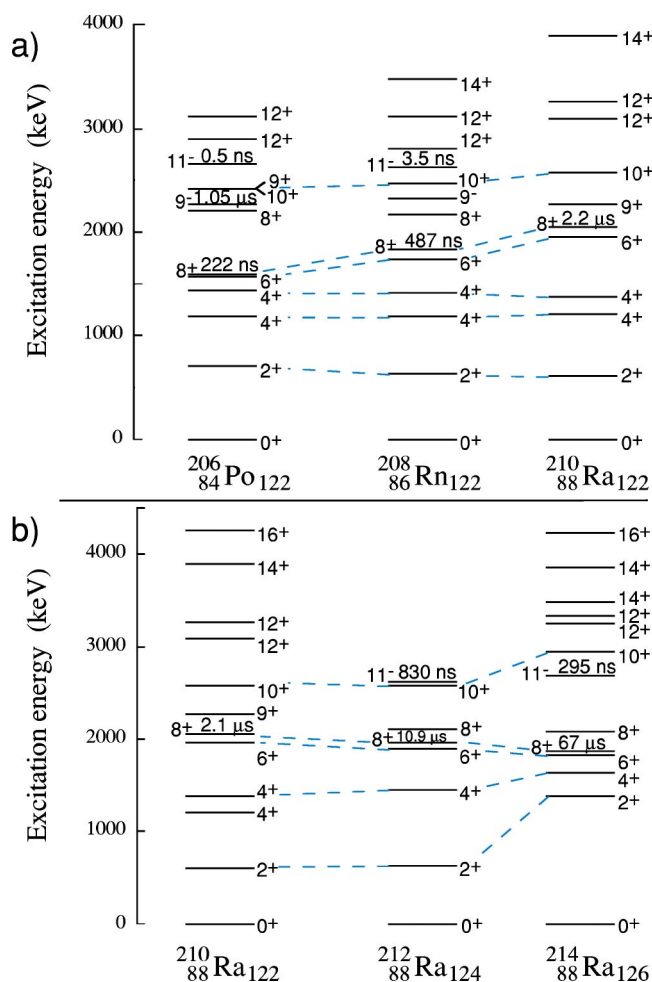


FIG. 7. Comparisons between even-even isotopes and isotones of ^{210}Ra with $Z > 82$ and $N < 126$. The level scheme for ^{210}Ra is derived from this experiment, while the neighboring isotones and isotopes are from Refs. [27,34,37].

and ^{210}Ra isotones suggests that the 4_2^+ is comprised of similar character (presumably predominantly $\pi 1h_{9/2}^n$), while the 4_1^+ is not.

Also shown in Fig. 8 are the 4_1^+ and 4_2^+ states of ^{204}Pb . In the neighboring $^{206}\text{Pb}_{124}$ isotope, the low-lying 4^+ states are primarily comprised of $(\nu f_{5/2})^{-1}(\nu p_{3/2})^{-1}$ and $(\nu f_{5/2})^{-2}$ configurations [45,46]. These same shell model orbitals would also be expected to comprise the low-lying 4^+ states in $^{204}\text{Pb}_{122}$. Due to the low energy of the neutron excitation in ^{204}Pb , one of the two low-energy 4^+ states in the $Z > 82$ isotones may be suggested as having a similar origin. The very similar energies of the 4_1^+ levels across the $N=122$ isotones with the weak branching from the 6^+ state suggests that the 4_1^+ states may be largely attributed to neutron excitations.

Neighboring nuclei of ^{210}Ra also exhibit secondary 8^+ states lying near the yrast 8^+ level. This second state is suggested to have a predominantly $\pi h_{9/2} \otimes \pi h_{7/2}$ configuration, with weak decays to the $8^+(\pi h_{9/2})^n$ yrast states due to the spin-flip nature of the transition. Decays from the yrast 10^+ level, suggested as predominantly $(\pi h_{9/2})^n \otimes 2^+$, are not observed to feed the 8_2^+ level in the neighboring nuclei. If a smooth trend for the 8_2^+ excitation energies is assumed, the

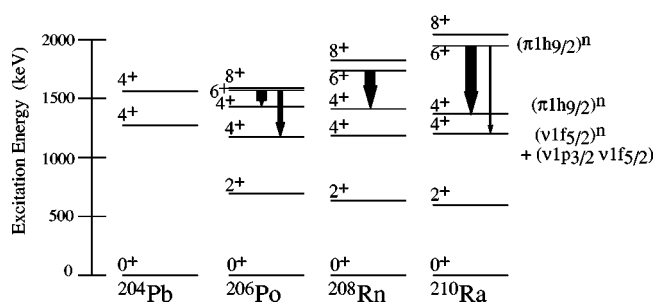


FIG. 8. Evolution of 4^+ neutron excitations along $N=122$. Arrows show transition probabilities from $6^+(\pi h_{9/2})^n$ excitations to the 4^+ levels. The relative strength of the decay is shown by the arrow width. The 4_1^+ state in the Po, Rn, and Ra isotones shown is suggested as a neutron excitation due to the weak $6^+ \rightarrow 4_1^+$ branching and similar excitation energy with semimagic ^{204}Pb . Data are from Refs. [35,37,43,44] and this work.

$8_2^+ \rightarrow 8_1^+$ transition would be ≈ 100 keV in ^{210}Ra . Due to the intense Ra x rays, γ -ray transitions ≤ 104 keV are impossible to suggest with confidence. Furthermore, due to the high proton number of ^{88}Ra , low-energy transitions are highly converted. It is possible that the slightly lower intensity of the $9^+ \rightarrow 8^+$ as compared to the $10^+ \rightarrow 9^+$ transition is due to unobserved branching to the 8_2^+ .

Clear evidence for additional isomeric states, such as the $11^-(\pi h_{9/2} \otimes \pi i_{13/2})$ or $9^-(\nu f_{5/2} \otimes \nu i_{13/2})$, was not observed in ^{210}Ra . Numerous weak isomeric transitions were observed, but could not be assigned unambiguously to ^{210}Ra . In addition, this experiment was only sensitive to half-lives less than ~ 5 ns or in the range of a few hundred nanoseconds to tens of microseconds. Decays with half-lives outside of these ranges would not have been observed.

Several transitions assigned to ^{210}Ra could not be placed in the level scheme; these transitions may feed isomeric states. For example, the 398 keV transition was easily observed in the prompt recoil- γ - γ coincidences, but was not present in the recoil-isomer gated γ spectrum. This would suggest that the 398 keV transition does not follow a decay path to the 8^+ isomer, possibly feeding a separate isomer.

The excitation energies for the 11^- isomers remain relatively constant across proton and neutron numbers at ~ 2.6 MeV. The isomer decays predominantly to the yrast 10^+ state, with weak branching to the yrast (isomeric) 8^+ levels. If a similar excitation energy is assumed in ^{210}Ra , this would suggest that the 11^- level lies only ~ 2.5 keV above the 10^+ state. None of the deexcitations below the 10^+ level, the 307 keV ($10^+ \rightarrow 9^+$), 217 keV ($9^+ \rightarrow 8^+$), nor the 524 keV ($10^+ \rightarrow 8^+$) were observed in the isomer detectors. Therefore, either (i) the 11^- level is not isomeric in ^{210}Ra , but due to the low energy and high conversion expected for the $11^- \rightarrow 10^+$ transition this decay was not identified in this experiment, or (ii) the 11^- level is isomeric in ^{210}Ra , but this experiment was not sensitive to the decay energy and/or lifetime.

A $9^-(\nu f_{5/2} \otimes \nu i_{13/2})$ neutron excitation is isomeric in ^{206}Po , but not ^{208}Rn , so it is not known if this state would be long lived in ^{210}Ra . In the isotope ^{206}Po , this level decays predominantly to the 8_2^+ level, with weaker branching to the 8^+ yrast state. The small energy difference (62 keV) between

the 9^- and 8_2^+ states may be the cause of the long lifetime. However, in the Rn isotone, the 9^- state is not isomeric, decaying only to the yrast 8^+ level in ^{208}Rn . The $J=9$ level at 2266 keV in ^{210}Ra is suggested to have positive parity based on intensity arguments. The 10^+ level at 2573 keV decays largely by an intense transition of 307 keV to the $J=9$ level at 2266 keV. As both the 518 ($I_\gamma \sim 100$) and 688 ($I_\gamma \sim 63$) transitions feed the 10^+ state, decays out of the state must have an approximately equal intensity. For this, both the $10^+ \rightarrow 9^-$ and the $9^- \rightarrow 8^+$ must have $M1$ multipolarity, as the conversion contribution with $E1$ is too small for the intensity balance.

B. ^{209}Ra

While this experiment focused on determining excitations in even-even ^{210}Ra , significant data were collected on ^{209}Ra as well.

Transitions feeding the proposed $13/2^+$ isomer and the low-lying negative-parity states of ^{209}Ra are observed in the prompt γ spectrum. Figure 5 shows the proposed level scheme for ^{209}Ra , with known level schemes from ^{205}Po [47] and ^{207}Rn [48]. All three isotones show remarkable similarities.

The low-lying 644, 765, and 371 keV transitions are also observed in the focal plane γ detectors. This suggests that these states are being partially fed from a high-lying isomer, possibly the $19/2^-[(\pi h_{9/2})_{8^+}^n \otimes \nu f_{5/2}]$ which is observed in neighboring odd- A Po and Rn isotopes. While short-lived isomeric states have not been measured in the isotone ^{207}Rn , in ^{209}Rn the $19/2^-$ decays by a low-energy $M1$ transition to a $17/2^-$ level which then decays by another low-energy $M1$ to a $15/2^-$ level which then branches to the $13/2^-$ and $11/2^-$ levels. If a similar decay path is assumed in ^{209}Ra , the high conversion probability and poor detection capability for the low-energy transitions may explain why they are not observed.

The excitation energy and half-life of the $13/2^+$ isomer are not known. In the Po and Rn isotopes with $N \leq 126$, this isomer decays by a single $M2$ transition to the $9/2^-$ first excited state. For lower neutron numbers, the excitation energy of the $13/2^+$ level decreases, increasing the isomer lifetimes. At still lower neutron numbers ($N=119$ for Po), the $13/2^+$ state lies below the $9/2^-$ state, increasing the isomer lifetimes significantly as the transition to the $5/2^-$ ground state has $M4$ multipolarity.

In ^{209}Ra , the $13/2^+$ isomer is expected to lie ~ 250 keV above the $9/2^-$ first excited state. For the Po and Rn isotones, the excitation energy of the $13/2^+$ level changes little; for $N=123$ the isomer lies at 1175 and 1174 keV, respectively, for Po and Rn, while for $N=121$ the isomer lies at 880 and 899 keV. A similar excitation energy is expected for $^{209}\text{Ra}_{121}$.

Along an isotone chain, half-lives for the $13/2^+$ isomer are three to four times shorter in Rn than Po. A similar trend

is expected in Ra; an upper limit of 181 μs , the $13/2^+$ isomer half-life in ^{207}Rn [49], may therefore be suggested for the isomeric decay in ^{209}Ra . If the isomer half-life decreases by a factor of 3–4 relative to ^{207}Rn , a half-life near 50 μs is expected. This experiment was designed to study isomers with half-lives of a few microseconds, and would thus be largely insensitive to the long lifetime of the $13/2^+$ isomer in ^{209}Ra .

V. CONCLUSIONS

In conclusion, we have measured prompt and delayed γ -ray spectra in the *trans*-Pb region with $A \approx 210$. Level schemes for both ^{210}Ra and ^{209}Ra have been constructed.

An 8^+ isomer in ^{210}Ra , presumably $\pi h_{9/2}^n$ in character, has been observed, and the half-life measured. The presence of this isomer allowed ^{210}Ra transitions to be selected from the prompt γ -ray spectrum.

The 8^+ isomeric decay in ^{210}Ra was compared to neighboring nuclei and interpreted in terms of the seniority scheme. A more extensive discussion of seniority systematics near closed shells will be published elsewhere [41]. Here we note only that the bowl-shaped behavior as a function of shell filling for $\Delta\nu=0$ yrast $B(E2)$ values in the seniority regime contrasts with the expected cap-shaped trend for seniority changing ($\Delta\nu=2$) yrast $B(E2)$ values and with the observed behavior of collective nuclei. As valence protons and neutrons are added beyond doubly magic nuclei, the seniority regime gives way to collective behavior and the pattern of $B(E2)$ values shown in Fig. 6(a) should transform to the usual cap-shaped trend. This contrasting behavior between seniority-dominated and collective regimes provides a new signature [41] of near-closed-shell, single- j configurations in exotic nuclei where the locations of magic numbers and the evolution of underlying shell structure are key issues of current and future concern.

Two isomers were also suggested in ^{209}Ra ; a short-lived ($\sim \mu\text{s}$) high-spin isomer which feeds into the low-lying negative-parity states, and a longer-lived (approximately tens of microseconds) $13/2^+(\nu i_{13/2})^{-1}$ state.

Very little is known about the light Ra isotopes with $N < 126$. This work extends the systematics to $N=121$, but studies of lower neutron numbers are necessary to address the issue of shape coexistence. Further studies of the even-even Ra isotopes, particularly $^{206}\text{Ra}(N=118)$ and $^{204}\text{Ra}(N=116)$ where the ground state deformation is predicted to change [21], will be essential for this understanding.

ACKNOWLEDGMENTS

Work supported by U.S. DOE under Grant Nos. DE-FG02-91ER-40609, DE-FG03-03NA-00081, and EPSRC (UK). P.H.R. would also like to acknowledge the Yale Flint and Science Development Funds.

- [1] R. G. Allatt *et al.*, Phys. Lett. B **437**, 29 (1998).
- [2] G. D. Dracoulis, A. P. Byrne, A. M. Baxter, P. M. Davidson, T. Kibédi, T. R. McGoram, R. A. Bark, and S. M. Mullins, Phys. Rev. C **60**, 014303 (1999).
- [3] G. D. Dracoulis, G. J. Lane, A. P. Byrne, A. M. Baxter, T. Kibédi, A. O. Macchiavelli, P. Fallon, and R. M. Clark, Phys. Rev. C **67**, 051301 (2003).
- [4] D. G. Jenkins *et al.*, Phys. Rev. C **62**, 021302 (2000).
- [5] A. N. Andreyev *et al.*, Nature (London) **405**, 430 (2000).
- [6] A. N. Andreyev *et al.*, Nucl. Phys. **A682**, 482c (2001).
- [7] A. N. Andreyev *et al.*, Phys. Rev. C **66**, 014313 (2002).
- [8] K. Van de Vel *et al.*, Phys. Rev. C **65**, 064301 (2002).
- [9] K. Van de Vel *et al.*, Phys. Rev. C **68**, 054311 (2003).
- [10] R. Julin, K. Helariutta, and M. Muikku, J. Phys. G **27**, R109 (2001).
- [11] T. Kibédi, G. D. Dracoulis, A. P. Byrne, and P. M. Davidson, Nucl. Phys. **A688**, 669 (2001).
- [12] M. O. Kortelahti, E. F. Zganjar, J. L. Wood, C. R. Bingham, H. K. Carter, K. S. Toth, J. H. Hamilton, J. Kormicki, L. Chaturvedi, and W. B. Newbolt, Phys. Rev. C **43**, 484 (1991).
- [13] P. M. Davidson, G. D. Dracoulis, T. Kibédi, A. P. Byrne, A. A. Anderssen, A. M. Baxter, B. Fabricius, G. J. Lane, and A. E. Stuchberry, Nucl. Phys. **A657**, 219 (1999).
- [14] F. G. Kondev *et al.*, Phys. Lett. B **512**, 268 (2001).
- [15] A. Melerangi *et al.*, Phys. Rev. C **68**, 041301 (2003).
- [16] F. G. Kondev *et al.*, Phys. Lett. B **528**, 221 (2002).
- [17] D. G. Jenkins *et al.*, Phys. Rev. C **66**, 011301 (2002).
- [18] E. Marshalek, L. Person, and R. K. Sheline, Rev. Mod. Phys. **35**, 108 (1963).
- [19] P. Möller and J. R. Nix, At. Data Nucl. Data Tables **26**, 165 (1981).
- [20] R. Bengtsson, P. Möller, J. R. Nix, and J. Zhang, Phys. Scr. **29**, 402 (1984).
- [21] P. Möller, J. R. Nix, W. D. Myers, and W. J. Swiatecki, At. Data Nucl. Data Tables **59**, 185 (1995).
- [22] K. Van de Vel *et al.*, Eur. Phys. J. A **17**, 167 (2003).
- [23] R. B. E. Taylor *et al.*, Phys. Rev. C **59**, 673 (1999).
- [24] N. Fotiadis *et al.*, Phys. Rev. C **55**, 1724 (1997).
- [25] K. Helariutta *et al.*, Eur. Phys. J. A **6**, 289 (1999).
- [26] A. M. Oros, K. Heyde, C. DeCoster, B. Decroix, R. Wyss, B. R. Barrett, and P. Navratil, Nucl. Phys. **A645**, 107 (1999).
- [27] Y. A. Akovali, Nucl. Data Sheets **76**, 127 (1995).
- [28] T. Kohno, M. Adachi, S. Fukuda, M. Taya, M. Fukuda, H. Taketani, Y. Gono, M. Sugawara, and Y. Ishikawa, Phys. Rev. C **33**, 392 (1986).
- [29] J. F. Cocks and JUROSPHERE Collaboration, J. Phys. G **25**, 839 (1999).
- [30] C. W. Beausang *et al.*, Nucl. Instrum. Methods Phys. Res. A **452**, 431 (2000).
- [31] J. J. Ressler *et al.*, Nucl. Instrum. Methods Phys. Res. B **204**, 141 (2003).
- [32] B. G. Ritchie, F. T. Avignone, H. K. Carter, R. L. Mlekodaj, and E. H. Spejewski, Phys. Rev. C **23**, 1717 (1981).
- [33] D. G. Raich, H. R. Bowman, R. E. Eppley, J. O. Rasmussen, and I. Rezanka, Z. Phys. A **279**, 301 (1976).
- [34] A. Artna-Cohen, Nucl. Data Sheets **66**, 171 (1992).
- [35] M. J. Martin, Nucl. Data Sheets **47**, 797 (1986).
- [36] R. S. Hager, and E. C. Seltzer, Nucl. Data, Sect. A **4**, 1 (1968).
- [37] E. Browne, Nucl. Data Sheets **88**, 29 (1999).
- [38] N. V. Zamfir and R. F. Casten, Phys. Lett. B **341**, 1 (1994).
- [39] I. Talmi, *Simple Models of Complex Nuclei* (Harwood Academic, Switzerland, 1993).
- [40] R. F. Casten, *Nuclear Structure from a Simple Perspective* (Oxford University Press, New York, 2000), p. 154.
- [41] J. J. Ressler *et al.*, Phys. Rev. C (to be published).
- [42] E. Browne, Nucl. Data Sheets **99**, 649 (2003).
- [43] A. M. Baxter, A. P. Byrne, G. D. Dracoulis, R. A. Bark, F. Riess, A. E. Stuchberry, M. C. Kruse, and A. R. Poletti, Nucl. Phys. **A515**, 493 (1990).
- [44] M. R. Schmorak, Nucl. Data Sheets **72**, 409 (1994).
- [45] W. W. True, Phys. Rev. **168**, 1388 (1968).
- [46] R. J. Lombard, Nucl. Phys. **71**, 348 (1965).
- [47] S. Rab, Nucl. Data Sheets **69**, 679 (1993).
- [48] J. Novak, Ph.D. thesis, Yale University; C. W. Beausang *et al.* (unpublished).
- [49] I. Rezanka, I. M. Ladenbauer-Bellis, and J. O. Rasmussen, Phys. Rev. C **10**, 766 (1974).